RSC Advances

ROYAL SOCIETY OF CHEMISTRY

www.rsc.org/advances

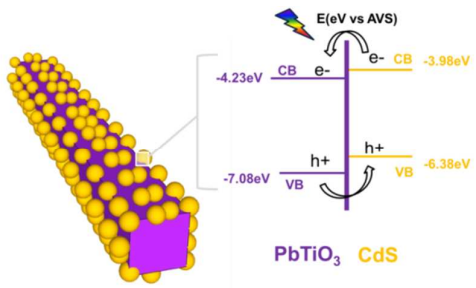

Single-crystal heterostructured $PbTiO_3$/CdS nanorods as efficient visible-light-driven photocatalysts for the degredation of methylene blue (MB).

RSC Advances

RSCPublishing

ARTICLE

Single-crystal Heterostructured $PbTiO_3$/CdS Nanorods with Enhanced Visible-light-driven Photocatalytic Performance

Cite this: DOI: 10.1039/x0xx00000x

Received ooth January 2012,
Accepted ooth January 2012

DOI: 10.1039/x0xx00000x

www.rsc.org/

Shan Jiang,[a] Zhaohui Ren,[*a] Ming Li,[a] Siyu Gong,[a] Yifeng Yu,[a] Jingyuan Pei,[b] Xiao Wei,[b] Ge Shen[a] and Gaorong Han[*a]

Single-crystal heterostructured $PbTiO_3$/CdS nanorods were fabricated by a hydrothermal process. In the composites, well-crystalline CdS nanoparticles grew on the surface of tetragonal perovskite $PbTiO_3$ nanorods and formed sharp $PbTiO_3$/CdS interfaces. It was revealed that the as-synthesized heterostructured $PbTiO_3$/CdS nanorods exhibited higher photocatalytic performance in degradation of MB under visible light irradiation over pristine $PbTiO_3$ nanorods and CdS nanoparticles. The enhanced performance is associated with the proper band alignment and promoted separation of photogenerated carriers by forming sharp interfaces between $PbTiO_3$ and CdS in the heterostructure. Our results suggest that the heterostructured $PbTiO_3$/CdS nanorods may be promising for high efficient visible-light-driven photocatalyst.

Introduction

In recent years, visible-light-driven photocatalysts have attracted much interest due to their high efficient photocatalytic activities using 46% of the incoming solar energy for water pollution treatment.[1-4] Among many approaches to developing novel photocatalysts, heterostructured design of semiconductor composites have been extensively studied because their physical and chemical properties can be largely optimised or modified by forming heterojunctions.[5-6] Due to its narrow band gap of 2.4eV,[7-8] high light harvesting efficiency in the visible region[9-10] and easy fabrication,[11] CdS becomes one kind of promising semiconductor building blocks for heterostructured visible-light-driven photocatalysts. Nevertheless, there are several issues that still limit their wide applications in environmental remediation and solar conversion.[12] For example, the CdS nanoparticles tend to aggregate, forming larger particles, which results in a reduced surface area and a higher recombination rate of photogenerated electron-holes.[13] In addition, CdS is easy to be corroded because the sulfide anion can be easily oxidized by photogenerated holes in aqueous media.[14] One way to prevent the self-oxidation of CdS is to couple the CdS nanoparticles with another semiconductor which have a lower but closely-lying conduction band (CB) and an appropriate valence band (VB), by forming heterostructured composite photocatalysts.[11] Up to now, several types of semiconductor nanomaterials, such as SnO_2,[15] TiO_2,[16] ZnO,[17] Fe_2O_3,[18] have been coupled with CdS to form heterostructured composites, which exhibited fascinating visible-light-driven photocatalytic performance. As the previous work discussed, the enhanced photocatalytic properties were ascribed to an effective separation of photogenerated electrons and holes via the heterostructured interfaces between CdS and other semiconductors,[19] where high quality interface with matched band alignment is desired to promoting charge carrier separation.[20]

Owing to flexible structure adoption and fruitful physical-chemical properties, perovskite oxide nanomaterials have been widely exploited as model photocatalysts in many studies.[21-24] Recently, we designed and synthesized single-crystal TiO_2/$PbTiO_3$ composite by a hydrothermal route, which demonstrated high visible-light catalytic performance as a result of the large-scale of sharp interfaces between TiO_2 and $PbTiO_3$.[25] However, the composite suffers low visible light absorption due to the wide band gap for TiO_2 and $PbTiO_3$, and the separation behaviour of photogenerated electron-hole pairs at the heterostructured interface is still unclear. Here, we further proposed the possible design of 1D heterostructured composite by forming well-crystallization sharp interfaces between $PbTiO_3$ nanorod and a narrow gap semiconductor nanomaterial, where proper band alignment, enhanced light harvesting and efficient separation of photogenerated carriers could be presumably achieved.

In this work, we used single-crystal perovskite $PbTiO_3$ nanorods as 1D nanoscale backbones for the secondary growth of CdS nanoparticles via a hydrothermal process. The composites demonstrate a superior photocatalytic activity for methylene blue compared to pure $PbTiO_3$ and CdS under

visible irradiation. Such performance has been discussed in terms of the sharp well-crystalline interfaces between $PbTiO_3$ and CdS with the balance of matching band alignment and high visible light harvesting efficiency, as well as the improved separation for the photogenerated carriers.

Experimental

Synthetic procedures

The synthesis of single-crystal perovskite $PbTiO_3$ nanorods is described in our previous report.[26] A typical synthesis of heterostructured $PbTiO_3$/CdS nanorods was as follows: 0.2g $PbTiO_3$ nanorods were well-dispersed in deionized water(30mL) under magnetic stirring and then cadmium chloride ($CdCl_2$) (1~5mM) and thiourea (1~5mM) were added into the suspension. The resulting mixture was continually stirred for 30min at room temperature to ensure the reaction had gone to completion and then added into a 50ml Telfon-lined stainless steel autoclave. The autoclave was maintained at 160°C for 12h, followed by cooling naturally to room temperature. The as-prepared samples were washed with deionized water and ethanol for several times, and subsequently air-dried at 60°C for 24h. The mass ratio of CdS in heterostructured $PbTiO_3$/CdS nanorods was about 5wt%-25wt%.

CdS nanoparticles were also prepared separately as a control experiment: 30mL aqueous solution of cadmium chloride ($CdCl_2$) (5mM) and thiourea (5mM) in deionized water was added into a 50ml Telfon-lined stainless steel autoclave. After magnetic stirring for 30 min, the autoclave was maintained at 160°C for 12h, followed by cooling naturally to room temperature. The as-prepared samples were washed with deionized water and ethanol for several times, and subsequently air-dried at 60°C for 24h.

Characterization

The morphology and the crystalline structure of the as-prepared heterostructured $PbTiO_3$/CdS nanorods were characterized with a Hitachi field emission scanning electron microscope (FESEM) instrument Model SU-70 at 3 kV and a FEI Tecnai G2 F20 S-TWIN high-resolution transmission electron microscope (HR-TEM) rated at 200 kV. X-ray powder diffraction (XRD) patterns were obtained by Thermo ARL X'TRA powder diffractometer with Bragg–Brentano geometry by Cu K α radiation (λ = 1.54056 Å) with 0.82 Å resolution. The specific surface area was determined according to the Brunauer-Emmett-Teller (BET) method using a Tristar Ⅱ3020 surface area and porosity analyser (Micrometrics). UV- visible absorption spectroscopy was recorded on UV-vis spectrophotometer (SHIMADZU UV-2550). The photoluminescence spectra were performed at room temperature using the 325 nm line of a continuous-wave He-Cd laser as the excitation source.

Photocatalytic Activity Measurement

In this study, we used the photocatalytic degradation of methylene blue (MB) under visible light to evaluate the photocatalytic activity of the as-prepared heterostructured $PbTiO_3$ /CdS nanorods, as MB is a typical model pollutant. A 300W Xe lamp with a UV cut-off filter (λ>400nm) was used as the visible light source and kept 20cm away from the photocatalytic reactor during the photocatalytic activity measurement. In a typical run of measurement, as-prepared catalyst (0.1g) was added into 100ml of MB solution (1×10^{-5} mol/L). Prior to the beginning of irradiation, the suspension was stirred for 40min to reach the adsorption-desorption equilibrium between the MB and the photocatalyst in dark. After that, the suspension was continuously stirred and exposed to light irradiation while the temperature of the suspension was kept at room temperature. Analytical samples were taken from the suspension every 0.5h and the photocatalyst powders were separated by centrifugation. The MB concentrations of the samples were measured by the UV-vis spectrophotometer and monitored by analysing the absorbance at 664nm. The $PbTiO_3$ nanorods and CdS nanoparticles were used in the control experiments.

Results and discussion

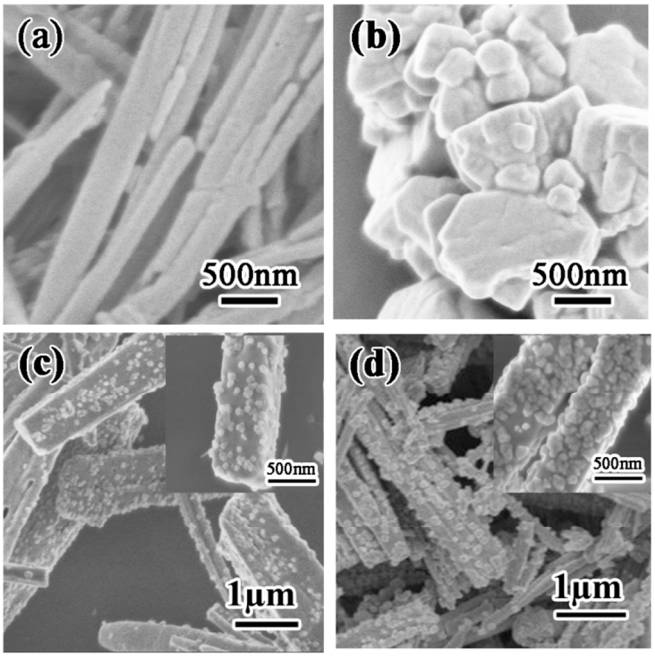

Figure 1 SEM images of (a) $PbTiO_3$ nanorods, (b) CdS nanoparticles, heterostructured $PbTiO_3$/CdS nanorods with mass ratio of (c) 15wt% and (d) 25wt%;

The morphology of the pristine $PbTiO_3$ nanorods, CdS nanoparticles and the heterostructured $PbTiO_3$/CdS nanorods was investigated by SEM, respectively. As shown in Figure 1a, the diameter of $PbTiO_3$ nanorods is about 200nm and the surface of the nanorods is clean. As shown in Figure 1b, CdS nanoparticles clearly aggregated with irregular shape and a wide size distribution from 50nm to 1μm. However, Figure 1c

and 1d show smaller CdS nanoparticles grew uniformly and tightly on the surface of $PbTiO_3$ nanorods in the heterostructured composite. With the increase of mass ratio for CdS, the diameter of the coated CdS nanoparticles increased from 20nm to 80nm.

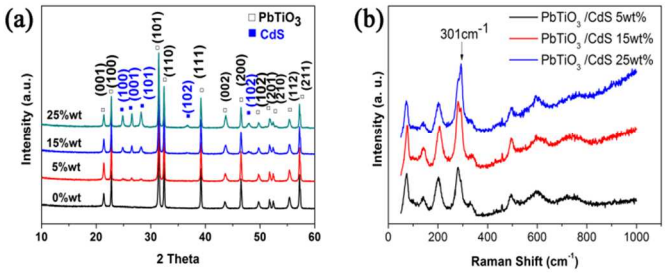

Fig 2. (a) XRD patterns of $PbTiO_3$ nanorods (the black line) and heterostructured $PbTiO_3$/CdS nanorods (the colour lines); (b) Raman spectra of the heterostructured $PbTiO_3$/CdS nanorods.

The phase and crystalline composition of the as-prepared samples were investigated by XRD. As shown in Figure 2a, all the peaks of the black curve can be indexed into the tetragonal perovskite structure of $PbTiO_3$ (JPCDS06-0452) and no other crystalline impurities were detected. The sharp diffraction peaks with a high intensity reveal high quality of crystallization for the samples. For the heterostructured $PbTiO_3$/CdS nanorods, the peaks marked by blue squares could be indexed into hexagonal greenockite CdS (JPCDS41-1049). The enhancement in the intensity of the peaks associated with different mass ratio of CdS can be ascribed to the improved crystallization and the increased amounts of CdS nanoparticles grown on the $PbTiO_3$ surface. Furthermore, the Raman spectra were collected to investigate the crystal phase and the microstructure of the heterostructured $PbTiO_3$/CdS nanorods. As shown in Figure S1, in the Raman spectrum of heterostructured $PbTiO_3$ nanorods, the peaks at 85, 151, 216, 287, 352, 437, 505, 651 and 750 cm^{-1} can be identified as the E(1TO), E(1LO), E(2TO), B1+E, A1(2TO), E(2LO)+A1(2LO), E(3TO) and A1(3TO) of perovskite $PbTiO_3$.[27] Aa shown in Figure 2b, in the Raman spectra of as-synthesized heterostructured $PbTiO_3$/CdS nanorods, an additional peak at 301cm^{-1} which can be ascribed to E(1LO)of CdS became stronger along with the increasing mass ratio of CdS.[28]

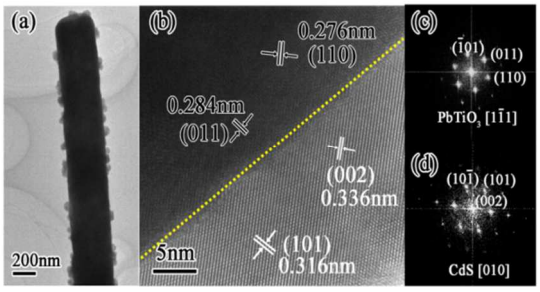

Figure 3. (a) TEM image of the heterostructured $PbTiO_3$/CdS 25wt% nanorod; the HRTEM image (b) and the corresponding fast Fourier transform (FFT) (c and d) of the heterostructured interface between $PbTiO_3$ and CdS.

The microstructure and morphology of the heterostructured $PbTiO_3$/CdS 25wt% nanorods were further investigated by TEM (Figure 3). As shown in Figure 3a, the CdS nanoparticles are about 80nm in diameter and growing on the surface of $PbTiO_3$ nanorods, which is consistent with SEM images. HRTEM image (Figure 3b) and the corresponding fast Fourier transform (FFT) (Figure 3c and d) of the interface region reveal the clear and sharp interface (dash line in the Fig 3b) with well-crystallization between $PbTiO_3$ and CdS. The lattice spacing of 0.276nm and 0.284nm for the nanorod could be indexed to the (110) and the (011) planes of tetragonal perovskite $PbTiO_3$. The lattice fringes of 0.336nm and 0.316nm are consistent with the spacing of (002) and (101) planes for the hexagonal greenockite CdS. TEM and HRTEM images further confirm the existence of crystalline CdS nanoparticles, which grew on the $PbTiO_3$ surface by forming unique sharp interface.

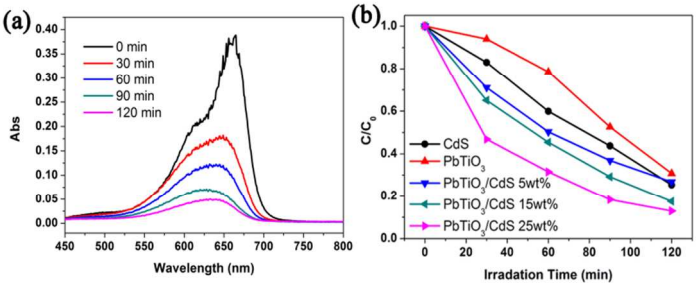

Figure 4. (a) Absorption spectra of the MB solution exposed to visible light irradiation for different time in the presence of heterostructured $PbTiO_3$/CdS 25wt% nanorods as photocatalyst. (b) Photocatalytic performances of different samples under visible light irradiation: CdS nanoparticles, the $PbTiO_3$ nanorods and the heterostructured $PbTiO_3$/CdS nanorods with increasing mass ratio of CdS.

In this work, the heterostructured $PbTiO_3$/CdS nanorods are utilized for the photocatalytic degradation of MB under visible light irradiation. As a comparison, the photocatalytic properties of the pristine $PbTiO_3$ nanorods and the CdS nanoparticles were also investigated. Figure 4a shows the UV-vis absorption spectra of the MB solution containing heterostructured $PbTiO_3$/CdS 25wt% nanorods during the photocatalytic degradation process. The absorption peaks at 612nm and 664nm correspond to dimers and monomers of MB, respectively.[29] The absorption peak at 664nm decreased rapidly as the irradiation time increased, indicating the degradation of MB. To clarify the absorption of MB molecules during the degradation process, we also investigated the degradation efficiency of the solution without visible light irradiation. As shown in Figure S2, the consumption of absorbed MB molecules on the surface of the catalysts was very little during the degradation reaction. As shown in Figure 4b, it is revealed that as the mass ratio of CdS increased, the photocatalytic activity of heterostructured nanorods would be enhanced. After irradiation for 120 min, the photocatalytic degradation efficiency reaches 87.1% for heterostructured $PbTiO_3$/CdS 25wt% nanorods, while 69.2% and 74.6% of MB were

degraded after the same irradiation time for the solution containing pristine $PbTiO_3$ and CdS, respectively.

Table 1 the first-order reaction rate of different samples.

Sample	K (min^{-1})
Blank	0.005
$PbTiO_3$	0.010
CdS	0.012
$PbTiO_3$/CdS 5wt%	0.011
$PbTiO_3$/CdS 15wt%	0.014
$PbTiO_3$/CdS 25wt%	0.017

Table 1 lists the first-order reaction rates of all the tested samples. The time evolution of the dye concentration can be reasonably accounted for by a pseudo-first-order model, represented by the following equation.[30]

$$\ln(C_0/C) = Kt \quad (1)$$

In this equation, C_0 is the dye concentration at time=0, C the concentration of dye at a time of t, K is the apparent first-order reaction rate, and t is the visible light exposure time. As listed in table 1, MB solution without adding catalyst was denoted as "Blank". And the first-order reaction rate of heterostructured $PbTiO_3$/CdS 25wt% nanorods shows a maximum of $0.017min^{-1}$, which is 1.4 times as that of CdS($0.012min^{-1}$) and 1.7 times as that of pure $PbTiO_3$($0.010min^{-1}$). The mechanism for the enhanced photocatalytic performance of heterostructured $PbTiO_3$/CdS nanorods can be discussed in terms of the following three aspects.

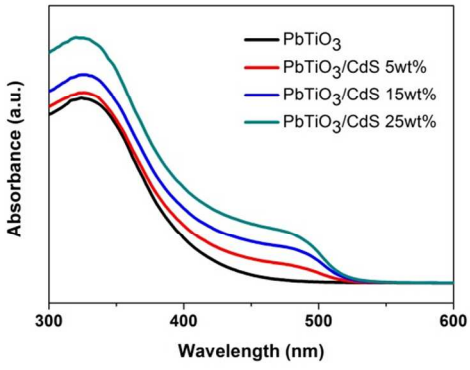

Fig. 5 UV-vis absorption spectra of $PbTiO_3$ nanorods and the heterostructured $PbTiO_3$/CdS nanorods.

Firstly, high-efficient light absorption in the visible region is critical for photocatalysts, the light absorption of $PbTiO_3$ nanorods and heterostructured $PbTiO_3$/CdS nanorods are shown in Figure 5. The absorption edge for pure $PbTiO_3$ nanorods is around 435nm, which is corresponding to the band gap.[23] In contrast, the heterostructured $PbTiO_3$/CdS nanorods demonstrate two absorption edges around 420 and 520nm, corresponding to the band edges of $PbTiO_3$ and CdS respectively.[9, 23] For the heterostructured $PbTiO_3$/CdS nanorods, an enhanced light absorption was achieved with the increasing amount of CdS nanoparticles on the surface of $PbTiO_3$ nanorods. Therefore, the heterostructured nanorods could absorb the visible light more efficiently, which is vital to the improvement of the visible-light-driven photocatalytic activity.

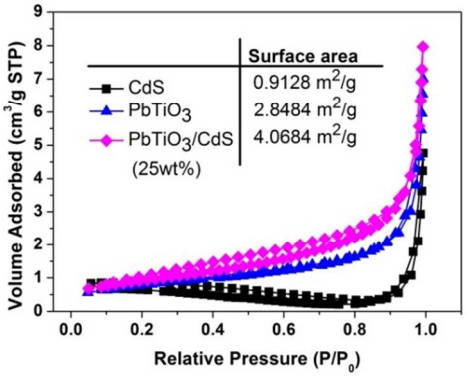

Figure 6. Nitrogen adsorption-desorption measurements and estimated BET surface areas of the $PbTiO_3$ nanorods, CdS nanoparticles and the heterostructured $PbTiO_3$/CdS 25wt% nanorods.

Secondly, the heterostructured $PbTiO_3$/CdS nanorods have larger surface area than those of $PbTiO_3$ nanorods and CdS nanoparticles. The BET surface areas of $PbTiO_3$ nanorods, CdS nanoparticles and heterostructured $PbTiO_3$/CdS 25wt% nanorods were calculated from the N_2 adsorption-desorption isotherms (Figure 6). CdS nanoparticles has been determined to have a low surface area of $0.5973m^2/g$, due to the agglomerate of the CdS nanoparticles through the hydrothermal process (Figure 1b). In contrast, the heterostructured $PbTiO_3$/CdS nanorods has a surface area of $4.0684m^2/g$, 42.8% higher than that of $PbTiO_3$ nanorods. The increase in the surface area could be ascribed to large scale of the heterostructured interfaces, and the rough surface of the heterostructured nanorods could provide more reaction sites for the photocatalytic activity.

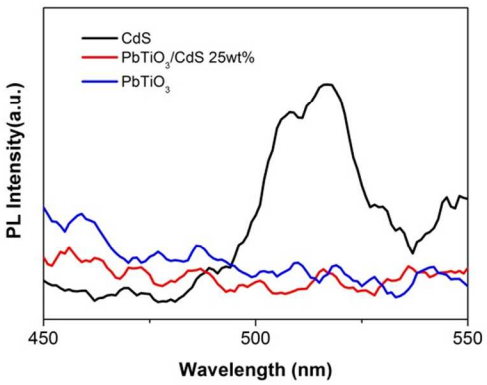

Figure 7. PL spectra of the $PbTiO_3$ nanorods, the CdS nanoparticles and heterostructured $PbTiO_3$/CdS 25wt% nanorods.

At last, the efficient separation of the photogenerated carriers at the heterostructured interface of the composite is another crucial factor to improve the photocatalytic activity. This could be confirmed by the photoluminescence (PL) spectra of the $PbTiO_3$ nanorods, CdS nanoparticles and heterostructured $PbTiO_3$/CdS 25wt% nanorods, as shown in Figure 7. In the PL spectrum of the $PbTiO_3$ nanorods, no emission peak could be observed, which may indicate the low content of surface defects in the pristine $PbTiO_3$.[31] As for to the PL spectrum of CdS, a band edge emission can be found at 516nm. Significant quenching of the band edge emission for CdS was observed after CdS nanoparticles were being combined to $PbTiO_3$ nanorods by forming sharp heterostructured interfaces, which implied that most of the photogenerated electro-hole pairs could be separated efficiently before the recombination process at the interface. The drastic quenching is reasonable, which could be ascribed to the proper band alignment between $PbTiO_3$ and CdS. Furthermore, the formation of well-crystalline heterostructured interface would facilitate the charge transfer and promote the photogenerated carriers separation at the interface.[15]

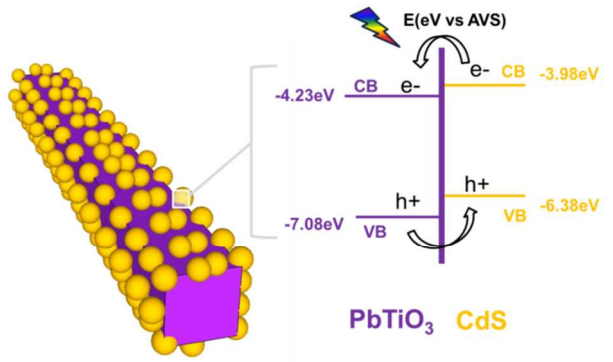

Figure 8. Schematic illustration for separation of the photogenerated carriers at the interface of the heterostructured $PbTiO_3$/CdS nanorods under visible light irradiation.

The schematic illustration for the separation of the photogenerated carriers in the heterostructured nanorods under visible light irradiation is shown in Figure 8. The calculated band edge (E_{CB}) for $PbTiO_3$ (-4.23eV) and CdS (-3.98eV) with respect to the absolute vacuum scale (AVS) is reported in previous study.[9,23] $PbTiO_3$ has a 0.25eV electric potential difference in the CB matching well with CdS, which is favourable for charge separation at the heterostructured interface. As shown in Figure 8, once the electrons in the VB of $PbTiO_3$ and CdS are excited to the CB under visible irradiation, the photo-induced electrons on the CB of CdS would transfer to the CB of $PbTiO_3$ while the photo-induced holes on the VB of the $PbTiO_3$ would transfer to the VB of CdS. Thus, the photogenerated electro-hole pairs could be separated more efficiently at the interface of the heterostructure and their recombination should be suppressed. In addition, the transportation of the photogenerated carriers through the heterostructured interface would be accelerated with the existence of electric potential difference.[32-33] On the other hand, the reducing size of CdS nanoparticles when forming heterostructured interface may shorten the diffusion pathway of the photogenerated charge carriers, which could facilitate the photocatalytic reaction in the $PbTiO_3$/CdS heterostructured nanorods.[19] Compared to single-phase photocatalysts, such heterostructure containing large scale of well-crystallization sharp interfaces possesses significant advantages in promoting the separation and transfer of the photogenerated carrier, eventually leading to an improvement in the photocatalytic performance.

Conclusions

Single-crystal $PbTiO_3$/CdS heterostructured nanorods were synthesized by a hydrothermal approach. With the size range of 20-80nm, the well-crystallized CdS nanoparticles grew on the single-crystal perovskite $PbTiO_3$ nanorods and formed large scale of sharp interfaces. The heterostructured $PbTiO_3$/CdS 25wt% nanorods demonstrated highest photocatalytic activity for the degradation of methylene blue (MB) under visible light irradiation, which could be attributed to the enhanced visible light harvesting efficiency, the larger surface areas of the heterostructures, large content of well-crystalline heterostructured interfaces, proper alignment of the band structure and efficient separation of the photogenerated carriers. These results show that the heterostructured $PbTiO_3$/CdS nanorods could be promising for high-performance visible-light-driven photocatalyst, and the findings may provide useful insights into the design of novel heterostructured photocatalyst.

Acknowledgements

This work was financially supported by the National Natural Science Foundation of China (No.51232006, 51472218). This work was financially supported by the Fundamental Research Funds for the Central Universities under Grant Nos. 2014XZZX005

Notes and references

[a] State Key Laboratory of Silicon Materials, School of Materials Science and Engineering, Cyrus Tang Centre for Sensor Materials and Application, Zhejiang University, Hangzhou 310027, P.R. China. E-mail: renzh@zju.edu.cn and hgr@zju.edu.cn。.

[b] Electron Microscope Center of Zhejiang University, Hangzhou, 310027, P. R. China

1 Z. G. Zou, J. H. Ye, K. Sayama, H. Arakawa, *Nature*, 2001, **414**, 625-627.

2 G. M. Wang, Y. C. Ling, H. Y. Wang, X. H. Lua, Y. Li, *J. Photoch. Photobio. C*, 2014, **19**, 35-51.

3 J. S. Luo, J. H. Im, M. T. Mayer, M. Schreier, M. K. Nazeeruddin, N. G. Park, S. D. Tilley, H. J. Fan, M. Grätzel *Science*, 2014, **345**, 1593.

4 X. B. Chen, S. H. Shen, L. J. Guo, and S. S. Mao, *Chem. Rev.*, 2010, **110**, 6503-6570.

5 K. Zhang and L. J. Guo, Catal. Sci. Technol., 2013, 3, 1672-1690.
6 L. Zhang, Y. G. Li, Q. H. Zhang and H. Z. Wang, *CrystEngComm*, 2013, **15**, 5986-5993.
7 E. Rabinovich and G. Hodes, *J. Phys. Chem. C*, 2013, **117**, 1611-1620.
8 S. B. Rawal, S. Bera, D. Lee, D. J. Jang and W. I. Lee, *Catal. Sci. Technol.*, 2013, **3**, 1822.
9 T. Lv, L. K. Pan, X. J. Liu and Z. Sun, *RSC Adv.*, 2012, **2**, 12706-12709.
10 W. Li, M. Y. Li, S. L. Xie, T. Zhai, M. H. Yu, C. L. Liang, X. W. Ouyang, X. H. Lu, H. H. Li and Y. X. Tong, *CrystEngComm*, 2013, **15**, 4212-4216.
11 Y. Qu, W. Zhou, L. Jiang and H. G. Fu, *RSC Adv.*, 2013, **3**, 18305-18310.
12 M. Luo, Y. Liu, J. C. Hu, H. Liu and J. L. Li, *ACS Appl. Mater. Interfaces* 2012, **4**, 1813−1821
13 Q. Li, B. D. Guo, J. G. Yu, J. R. Ran, B. H. Zhang, H. J. Yan, and J. R. Gong, *J. Am. Chem. Soc.*, 2011, **133**, 10878-10884.
14 Y. L. Min, G. Q. He, Q. J. Xu and Y. C. Chen, *J. Mater. Chem. A*, 2014, **2**, 2578-2584.
15 J. Pan, J. T. Li, Z. L. Yan, B. H. Zhou, H. S. Hua and X. Xiong, *Nanoscale*, 2013, **5**, 3022-3029.
16 Y. Medina-Gonzalez, W. Z. Xu, B. Chen, N. Farhanghi and P. A. Charpentier, *Nanotechnology*, 2011, **22**, 065603.
17 G. M. Wang, X. Y. Yang, F. Qian, J. Z. Zhang, and Y. Li, *Nano Lett.*, 2010, **10**, 1088-1092.
18 Y. Shi, H. Y. Li, L. Wang, W. Shen, and H. Z. Chen, *ACS Appl. Mater. Interfaces*, 2012, **4**, 4800-4806.
19 R. Marschall, *Adv. Funct. Mater.*, 2014, **24**, 2421-2440.
20 X. B. Chen, S. H. Shen, L. J. Guo, and S. S. Mao, Chem. Rev., 2010, 110, 6503-6570.
21 J. Ng, S. P. Xu, X. W. Zhang, H. Y. Yang, D. D. Sun, *Adv. Funct. Mater.*, 2010, **20**, 4287-4294.
22 H. W. Bai, J. Juay, Z. Y. Liu, X. X. Song, S. S. Lee, D. D. Sun, *Appl. Catal. B*, 2012, **125**, 367-374.
23 L. Li, Y. L. Zhang, A. M. Schultz, X. Liu, P. A. Salvador and G. S. Rohrer, *Catal. Sci. Technol.*, 2012, **2**, 1945-1952.
24 S. Jiang, Z. H. Ren, S. M. Yin, S. Y. Gong, Y. F. Yu, X. Li, X. Wei, G. Xu, G. Shen and G. R. Han , *ACS Appl. Mater. Interfaces*, 2014, **6**, 10935-10940.
25 Y. F. Yu, Z. H. Ren, M. Li, S. Y. Gong, S. M. Yin, S. Jiang, X. Li, X. Wei, G. Xu, G. Shen and G. R. Han, *CrystEngComm*, 2015, **17**, 1024-1029.
26 Z. Y. Liu, Z. H. Ren, Z. Xiao, C. Y. Chao, X. Wei, Y. Liu, X. Li, G. Xu, G. Shen and G. R. Han, *Small*, 2012, **8**, 2959-2963.
27 S. Y. Gong, Z. H. Ren, S. Jiang, M. Li, X. Li, X. Wei, G. Xu, G. Shen and G. R. Han, *J. Phys. Chem. C*, 2014, **118**, 5486-5493.
28 R. R Prabhu and M. A. Khadar, *Bull. Mater. Sci.*, 2008, **31**, 511-515.
29 J. S. Lee, K. H. You, and C. B. Park, *Adv. Mater.*, 2012, **24**, 1084-1088.
30 S. M. Yin, H. Tian, Z. H. Ren, X. Wei, C. Y. Chao, J. Y. Pei, X. Li, G. Xu, G. Shen and G. R. Han, *Chem. Comm.*., 2014, **50**, 6027-6030.
31 Y. Yang, X. H. Wang, C. K. Sun and L. T. Li, *J. Am. Ceram. Soc.,* 2008, **91**, 3820-3822.
32 A. Kar, S. Kundu and A. Patra, *RSC Adv.*, 2012, **2**, 10222-10230.
33 M. D. Han, T. Sun, P. Y. Tan, X. F. Chen, O. K. Tana and M. S. Tse, *RSC Adv.*, 2013, **3**, 24964-24970.

